Two-dimensional superconductivity driven by interfacial electron-phonon coupling in a $BaPbO_3/BaBiO_3$ bilayer

S. Di Napoli [1,2] C. Helman [2,3] A. M. Llois,[1,2] and V. Vildosola [1,2,*]

[1]*Departamento de Física de la Materia Condensada, Gerencia de Investigación y Aplicaciones, Comisión Nacional de Energía Atómica, Av. General Paz 1499, (1650) San Martín, Pcia. de Buenos Aires, Argentina*

[2]*Instituto de Nanociencia y Nanotecnología, Comisión Nacional de Energía Atómica and Consejo Nacional de Investigaciones Científicas y Técnicas, 1650 San Martín, Argentina*

[3]*Centro Atómico Bariloche and Instituto Balseiro, Comisión Nacional de Energía Atómica, 8400 S. C. de Bariloche, Argentina*

(Received 16 November 2020; revised 12 March 2021; accepted 4 May 2021; published 18 May 2021)

The recent discovery of two-dimensional (2D) superconductivity at the interface of $BaPbO_3$ (BPO) and $BaBiO_3$ (BBO) has motivated us to study in depth the electronic and structural properties and the relation between them in this particular heterostructure, by means of first-principles calculations. Our results indicate that the breathing distortions, the charge ordering, and the semiconducting behavior that characterize the parent compound BBO in its bulk form are preserved at the innermost layers of the BBO side of the BPO/BBO bilayer. On the other hand, at the interface, there is a partial breaking of the breathing distortions with a concomitant charge transfer between the interfacial Bi ions and the on top BPO layer. We show that two types of carriers coexist at the interface, the delocalized three-dimensional-like *sp* states coming from Pb ions and the quasi-2D *s* states from the Bi ones. We obtain a substantial electron-phonon coupling between the 2D Bi states with the interfacial stretching phonon mode and a large density of states that can explain the critical temperature experimentally observed below 3.5 K. We hope these findings will motivate future research to explore different interfaces with charge-ordered semiconductors such as BBO in order to trigger this fascinating 2D behavior.

DOI: 10.1103/PhysRevB.103.174509

In recent decades, the scientific community has devoted a great effort to finding emerging properties at the interfaces of oxide heterostructures with the aim of diversifying the functionalities of existing electronic devices. In oxide materials, the covalency of the bonds and the fact that the crystal structures are conducive to varying the chemical composition enable the possibility of controlling different electronic degrees of freedom and the interrelations among them and/or with the crystal structure and its dynamics. This is a clue for designing new devices with novel technologies in which the interface between the constituent materials plays a fundamental role. Different physical phenomena such as long-range orders, superconductivity, and metal-insulator transitions can be exploited for this purpose.

In particular, the discovery of interfacial superconductivity in oxide heterostructures has caught much attention. First, it was demonstrated that superconductivity can occur at the interface between two band insulators such as $LaAlO_3$ and $SrTiO_3$ [1]. Later, it was the turn of the strongly correlated cuprates La_2CuO_4 and $LaSrCuO_4$, for which high-T_c interfacial superconductivity was reported [2], and it can occur even at a sole CuO_2 plane [3]. Very recently, two-dimensional (2D) superconductivity was probed at the $FeSe/SrTiO_3$ interface [4] independent of the thickness of the FeSe film.

Interestingly, 2D superconductivity was also observed at the $BaPbO_3/BaBiO_3$ bilayer [5]. Separately, $BaBiO_3$ (BBO) is a charge-ordered Peierls-like semiconductor while $BaPbO_3$ (BPO) films are metallic, but the emerging 2D superconductivity remains unclear. The 2D superconducting T_c reported for the BPO/BBO bilayer reached up to 3.5 K depending of the thickness of the BPO layer. In this work, we give insight into the detailed electronic structure, structural reconstructions, and interfacial vibrations of this bilayer by means of first-principles calculations.

The phase diagram of bulk BBO is very rich and deserves a brief description in order to understand the properties at the interface. Among the most outstanding features is the fact that it becomes superconducting under hole doping in the vicinity of a charge-density wave ordered phase. Despite the absence of magnetic instabilities in the parent compound, the critical temperature (T_c) can be as high as 32 K [6] for $Ba_{0.6}K_{0.4}BiO_3$ (BKBO) when K replaces Ba sites which are not in the BiO_2 superconducting plane, or it can reach up to 13 K [7] for $BaPb_{0.7}Bi_{0.3}O_3$ (BPBO) when Pb substitutes Bi.

Undoped BBO crystallizes in a double perovskite type structure. The formula unit forces the Bi atom to have the formal valence +4; however, due to the lone pair effect, this valence state is unstable so that, at low temperatures, the system develops an insulating charge ordered state with alternated Bi^{+5}-Bi^{+3} sites. In reality, the difference in charge between both Bi sites is much less than the formal valence due to hybridization and screening effects [8,9]. Actually, Bi-O bonds can be described by spatially extended hybridized 6*s*-2*p* orbitals [10,11]. The disproportionate charge induces structural distortions characterized by the tilting of the

*vildosol@tandar.cnea.gov.ar

octahedra and especially by the breathing modes of the Bi-O bonds. As the temperature goes down, the system undergoes several transitions in the crystal structure, losing its symmetry, going through cubic ($T > 750$ K), rhombohedral (405 K $< T <$ 750 K), and monoclinic ($T < 405$ K) phases [12]. Under hole doping (above a certain optimal value), there is no need to avoid the +4 valence state; the system turns simple cubic, metallic, and more important, superconducting below T_c. The physical nature of the superconducting phase has been debated for several decades. Recently, it has been demonstrated through angle-resolved photoemission spectra (ARPES) that the large electron-phonon coupling, in particular with those phonon modes related to the breathing distortions, can account for the high T_c [13]. It has also been confirmed that it is necessary to go beyond local or semilocal functionals as the local density approximation or the general gradient approximation to account for the long-range exchange interactions and that density functional theory (DFT) calculations that take into account the nonlocal Hartre-Fock exchange interactions by means of screened hybrid functionals can describe the physics correctly [9,14].

On the other hand, bulk BPO, the other compound of the bilayer, is monoclinic at low T and pure BPO films were reported to be metallic [5,15]. The valence +4 that imposes the perovskite formula unit for the Pb site implies that the 6*s* and 6*p* bands are practically empty. Unlike what happens in BBO, there is only one crystal site type for Pb. It was suggested that the 2D superconductivity at the BBO/BPO interface was induced by the interfacial strain and that BPO acts as a dopant.

In this work, we provide a microscopic description of the electronic structure at the interface of this bilayer and study the coupling of the interfacial electronic states with the lattice dynamics. We show that at the BPO/BBO interface there is a partial breaking of the BBO charge order, which gives rise to 2D electronic states that present a strong coupling with interfacial phonons. This mechanism of generating 2D electronic states is similar to the one predicted for the Bi terminated (001) surface of pure BBO [16].

We perfom DFT calculations including a fraction of nonlocal Hartre-Fock exchange interactions through the Heyd-Scuseria-Ernzerhof (HSE06) functionals [17,18] as implemented in the Vienna *ab initio* package (VASP) [19–21].

X-ray diffraction (XRD) studies reported in Ref. [5] indicate that BBO grows completely relaxed on $SrTiO_3$ substrates, while there is a clear strained growth of the BPO layer on BBO. Based on this experimental evidence, we simulate the BPO/BBO bilayer considering a supercell in the monoclinic crystal structure of BBO using the experimental lattice parameters [12] and relaxing the internal positions. The description of all the studied slabs BPOi/BBOj with different values of i and j is presented in the Supplemental Material [21]. In this notation, the supercell is built along the (001) direction, i is the number of BPO layers, and j the corresponding number for BBO. The supercell is rotated 45° with respect to the simple cubic single perovskite and contains two Bi or two Pb sites per layer.

In order to properly describe the breathing distortions in BBO, a rather dense k mesh is necessary [22]. The relaxation of internal positions of the different slabs is performed within the Perdew-Burke-Ernzerhof (PBE) [24] functional. In the Supplemental Material, we show that PBE gives reasonable results for the breathing distortions and the charge disproportionation[1] as compared to the HSE outcome. Its main drawback is the description of the bandwidths and the electronic band gap, so we use the HSE functionals at the electronic level for these large supercells.

In Fig. 1(a), we show half of the supercell considered for the BPO2/BBO6 slab. Layers indicated as 1, 2, and 3 correspond to half of the BBO part, with layer 1 being the interfacial Bi layer while layer 3 is the innermost one. In Figs. 1(b), 1(c) and 1(d), the crystal and electronic reconstructions after relaxation of the internal parameters can be observed. Figure 1(b) shows an enlargement of the Bi-O octahedra at layer 3. The Bi^{+3}-O and Bi^{+5}-O distances, $d_1 =$ 2.30 and $d_2 = 2.16$ Å, respectively, present very similar values to the ones obtained for bulk BBO (see Table S1 in the Supplemental Material). On the other hand, Fig. 1(c) shows the crystal structure at the interface. The interfacial distance Bi^{+3}-O, d_3, shrinks about 5% with the respect to the innermost values d_1, as indicated with the blue arrow in the figure, while the interfacial Bi^{+5}-O, d_4, remains practically unchanged. This partial suppression of the breathing distortion at the interface is in line with the electronic reconstruction that can be observed in the layer-by-layer projected density of states (PDOS) of Fig. 1(d). At the top panel, the metallic *sp*-Pb PDOS is shown. At the botton, the *s*-Bi^{+3} and *s*-Bi^{+5} PDOS of layer 3 indicate that the slab holds the semiconducting behavior away from the interface. At this layer, the *s*-Bi^{+3} band is full while the *s*-Bi^{+5} one is empty. Similarly, this disproportionate charge among the Bi sites survives at layer 2. However, at the interface, layer 1 turns out to be metallic due to a charge transfer between Bi^{+3} and the top BPO layer. Curiously, the *s*-Bi^{+5} band stays empty.

Figure 2 (top panel) depicts the band structure calculated for the BPO2/BBO6 slab. Here, the *s*-Bi^{+3} character of the Bi atom at layer 1 is highlighted in blue. The *s*-Bi^{+5} character for the same layer is in red and the total *sp*-Pb character is in green. It is important to remark that while the *s*-Bi^{+3} states at Fermi energy (E_F) are quasi-2D, since only the states lying at layer 1 contribute to E_F, the *sp*-Pb bands are more delocalized and 3D like. The calculations done for the BPO4/BBO6 slab indicate that all the Pb atoms contribute equally to E_F. At the botton of Fig. 2, we show the calculated charge density for the bands crossing E_F. The charge density of the hole band with more *s*-Bi^{+3} character is centered around the interfacial Bi^{+3} sites while the electron band with *sp*-Pb character is clearly more delocalized with substantial weight at the oxygens of the BBO part.

Interestingly, comparing the band structure of the BPO2/BBO4, BPO2/BBO6, and BPO2/BBO8 (see the Supplemental Material), the height of the hole pocket does not significantly change with the number of BBO layers, as long as they are more than four. The reason is that the partial suppression of the charge order is a 2D effect at the interface. On the other hand, the doping effect of the BPO slab is a bit

[1]We assess the charge disproportionation through a Bader charge analysis [23].

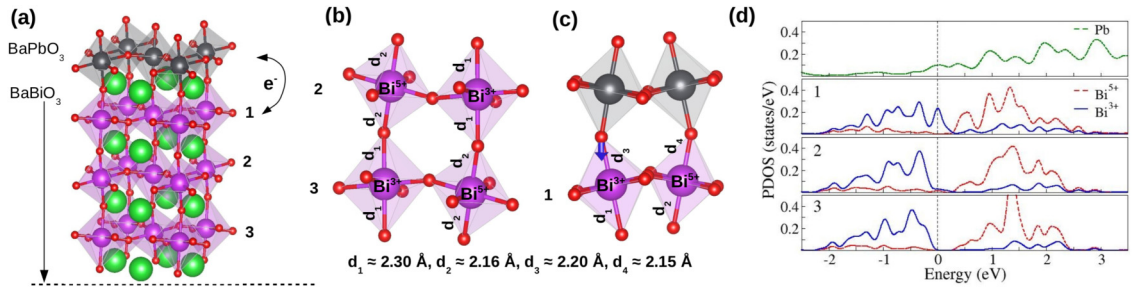

FIG. 1. (a) Schematic representation of the $BaBiO_3/BaPbO_3$ interface. We show half of the structure used in our simulations. Numbers 1–3 represent the plane number. [(b), (c)] Octahedral environment of Bi atoms belonging to the bulk and interface regions, respectively. (Green, Ba; magenta, Bi; red, O; and gray, Pb atoms). (d) Bi (*s*) and Pb (*sp*) partial density of states (PDOS) projected onto the planes labeled in panel (a).

more sensitive with its width; as the BPO part gets wider, the doping on the BBO one becomes more effective. The sizes of both the hole and electron pockets increase with the width of the BPO side, as can be observed by comparing BPO2/BBO6 with BPO4/BBO6 in the Supplemental Material. We will come back to this point when we discuss the electron-phonon coupling.

Both materials, BPO and BBO, have been predicted to have large topological gaps both in the electron and hole doping regimes [25,26]. In view of these properties, we have assessed the role of spin-orbit (SO) coupling on these interfacial effects of the bilayer. As shown in the Supplemental Material, we observe the opening of gaps when the SO is turned on, but these gaps are far away from the Fermi level of the interface studied here. Thus, we conclude that the topological properties of these materials do not affect the electronic behavior of this bilayer.

We now study the coupling of these interfacial states with the lattice dynamics. Yin *et al.* have shown that for doped BBO in its bulk form, the three phonon modes that couple more strongly to the electrons are the breathing, the stretching (ST), and the ferroelectric (FE) modes [14]. At the BPO/BBO interface, the 3D breathing mode is obviously no longer operative and, therefore, we study the effect of the other two modes and estimate their contribution to the electron-phonon coupling.

As proposed in Refs. [27,28], and described in the Supplemental Material, the electron-phonon matrix elements can be estimated at a given wave vector q and phonon mode ν, through a frozen phonon approach directly from the shift of the bands calculated for a proper supercell, as long as q is commensurate with the lattice.

In the optimally doped bulk BBO, the undistorted crystal is a single simple cubic perovskite. As shown before, in the bilayer studied here, the breaking of charge order at the interface is partial so that the system remains in a double perovskite configuration. The simulated supercells allow us to estimate the electron-phonon matrix elements for the interfacial ST and FE modes and compare them with the bulk BBO ones, at the wave vector $\pi/a(1,1)$ of the single perovskite structure, to assess their relative strength.

The frozen phonon calculations are performed both with the PBE and HSE functionals (see the Supplemental Material for a detailed comparison). In Fig. 3, we plot the calculated

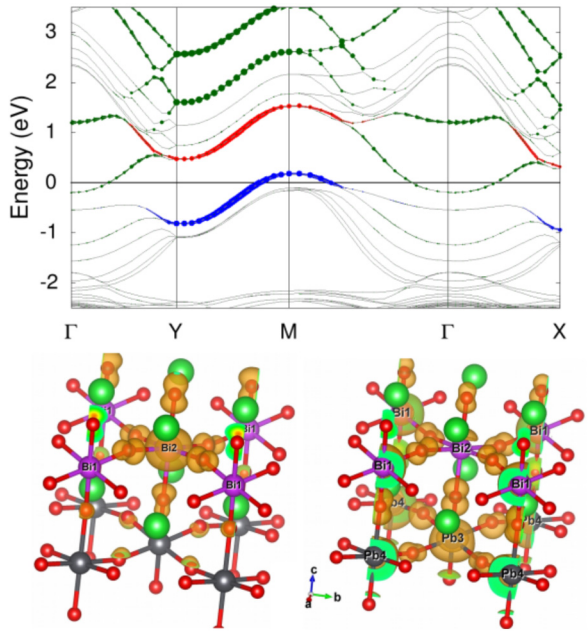

FIG. 2. (Top) HSE band structure of the BPO2/BBO6 heterostructure. The *s* character of interfacial Bi^{5+} (red circles) and Bi^{3+} (blue circles) and the *sp* character of Pb (dark green circles) are shown. (Bottom) Charge density obtained from the states crossing the Fermi level from below (left) and from above (right) corresponding to charge density mainly centered at the interfacial Bi^{3+} and Pb (and Bi^{5+}) atoms, respectively.

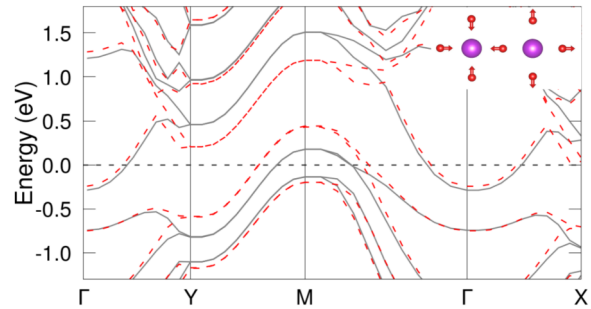

FIG. 3. HSE bandsstructures of the BPO2/BBO4 heterostrusture in the undistorted (black solid line) and ST (dashed red lines) distortions. In the right insets, the ST frozen phonon displacements are shown. The oxygen atoms's displacements considered are 0.044 Å.

HSE band structure of the BPO2/BBO4 slab in its relaxed structure (black solid line) together with the ones obtained for the ST (red dashed lines) distortions. The effect of the FE interfacial distortion is negligible (see the Supplemental Material). On the other hand, there is a substantial change in the electronic bands that cross E_F for the ST mode, especially for the hole pocket surrounding the M point, which is the one with more s-Bi^{+3} character. For the frozen-phonon distortions, we consider a small atomic displacement of $|u| \approx 0.044$ Å as in Ref. [14]. The other bands at E_F come from the nearly empty Pb ones for which we have not observed any sizable electron-phonon coupling.

The estimated matrix element for the ST mode at the M point is 4.6 eV/Å with PBE, and turns to 5.9 eV/Å with HSE. The corresponding values of these shifts for the optimally doped bulk BBO are 5.1 and 8.9 eV/Å with PBE and HSE, respectively [14]. Two things are important to remark. On one hand, the difference between the PBE and HSE for the interfacial ST mode is not as important as for the doped bulk BBO. This is probably due to the fact that at the interface, the breaking of charge ordering is only partial. Second, the interfacial ST electron-phonon matrix elements for the bilayer are substantial. They are smaller but of the same order as the strongest coupling in bulk BBO. It is noteworthy to say that we also obtain a value of 4.6 eV/Å within PBE for the matrix element of the thicker BPO4/BBO6 slab. The main difference between the two slabs is mainly the density of states (DOS) at E_F per spin, $N_0^{\uparrow}$, that is larger for the thicker one, being 1.25 and 1.90 states/eV within PBE, respectively.

Then, the contribution to the electron-phonon coupling λ from this interfacial stretching mode (IST), $\lambda_{\rm IST}$, is obtained by performing the double δ sum in Eq. (S1) of the Supplemental Material, with the matrix elements calculated along the full Brillouin zone. Gaussian functions have been used to simulate the δ. The phonon frequency of the IST mode, $\omega_{q\rm IST}$ with $q = 0$, has been estimated by a direct approach within the frozen phonon approximation, through which the changes in total energy are calculated in real space by slightly displacing the atoms from their equilibrium positions in the interfacial ST mode, giving $\omega_{0,\rm IST} \approx 0.059$ eV. [2]

As compared with the strongest electron-phonon coupling in the optimally doped bulk BBO, that is, the breathing mode contribution (bBR),[3] we obtain $\lambda_{\rm IST} \simeq \lambda_{b\rm BR}/3$ for a wide range of Gaussian smearing σ values (0.002 Ry $\lesssim \sigma \lesssim$ 0.02 Ry) and well-converged k-point grids. However, we remark that the absolute value that comes out of the double δ sum is sensitive to σ. The reported values for $\lambda_{b\rm BR}$ and total $\lambda_{\rm 3D}$ for the optinally doped BBO are 0.3 [28,29] and 0.34 [29], respectively. If we consider that total electron-phonon coupling at the interface of the smallest simulated slab is $\lambda_{\rm 2D} = \lambda_{\rm 3D}/3$, within PBE $\lambda_{\rm 2D} = 0.11$.

Resorting to the simplified expression

$$\lambda = N_0^{\uparrow} \langle\langle g^2 \rangle\rangle / M \langle\langle \omega^2 \rangle\rangle, \tag{1}$$

where $\langle\langle g^2 \rangle\rangle$ and $\langle\langle \omega^2 \rangle\rangle$ are the properly averaged square of the coupling matrix elements and phonon frequencies as described in Ref. [30] and assuming that the frequencies do not significantly vary for slabs with different sizes, we can rescale the PBE value for $\lambda_{\rm 2D}$ of the thinner slab to the corresponding thicker one for the BPO4/BBO6 case withing HSE, following the method suggested in Ref. [14]:

$$\lambda_{\rm 2D}^{\rm HSE,thick} = \lambda_{\rm 2D}^{\rm PBE,thin} \frac{N_{\rm HSE,thick}^{\uparrow} \langle\langle g^2 \rangle\rangle_{\rm HSE}}{N_{\rm PBE,thin}^{\uparrow} \langle\langle g^2 \rangle\rangle_{\rm PBE}}, \tag{2}$$

where $N_{\rm PBE,thin}^{\uparrow}$ is the calculated DOS at E_F for the thinner BPO2/BBO4 slab within PBE that is equal to 1.25 states/eV and $N_{\rm HSE,thick}^{\uparrow}$ is the corresponding one for the BPO4/BBO6 slab within HSE, equal to 2.5 states/eV. The rescaling of the averaged squared coupling matrix elements is done considering the calculated values 4.6 eV/Å (PBE) and 5.9 eV/Å (HSE), correspondingly. We recall that this coupling shows no sensitivity to the width of the BPO as mentioned before. By doing this rescaling, we obtain that the $\lambda_{\rm 2D}^{\rm HSE,thick} = 0.36$.

Considering the modified McMillan equation for the superconducting critical temperature,

$$T_c = \frac{\omega_{\log}}{1.2} \exp\left(-\frac{1.04(1+\lambda)}{\lambda - \mu^*(1+0.62\lambda)} \right), \tag{3}$$

and taking $\omega_{\log} = 450$ K and $\mu^* = 0.1$, the same parameters reported in Ref. [14] for BBO bulk,[4] our obtained value of $\lambda_{\rm 2D}$ gives rise to $T_c \sim 1$ K, which is of the same order of magnitude of the experimentally observed T_c for the BPO/BBO bilayer. Thicker BPO bilayers are expected to increase even more the DOS at E_F and, concomitantly, enlarge T_c.

The main message of this work, then, is that there is a substantial coupling between the electrons and the interfacial stretching vibrations and a large $N_0^{\uparrow}$ that can explain the experimentally observed 2D superconductivity below 3.5 K. In Fig. 4, we show a schematic representation of the evolution of T_c along the BBO family of superconductors that can be qualitatively explained by Eq. (3). In Ref. [14], $\lambda_{\rm 3D} \approx 1$ was calculated within HSE and confirmed experimentally through ARPES [13]. Interestingly, the decrease of T_c from BKBO to BPBO can be obtained by just rescaling the DOS at E_F (going from 0.44 to 0.26 states/eV [11]) while keeping $\langle\langle g^2 \rangle\rangle$ fixed

[2]We also confirm this value from the second derivatives of the energy with respect to atomic displacements (Hessian matrix) to obtain all the vibrational frequencies of the bilayer. This is done by setting IBRION = 5 in the VASP calculations. It is worth recalling that within our supercell the matrix elements for $q = 0$ wave vector can be mapped to the $[\frac{\pi}{a}(1,1)]$ point of the single cubic perovskite.

[3]We have calculated the breathing mode contribution to the electron-phonon coupling of the doped bulk BBO ($\lambda_{b\rm BR}$) within the same approximation as for $\lambda_{\rm IST}$, obtaining the matrix elements from a frozen phonon approach along the full Brillouin zone. We have considered a $2 \times 2 \times 2$ face-centered cubic (fcc) supercell, the doping effect was simulated by the virtual crystal approximation, and the atomic displacements of the oxygens in the breathing mode was 0.044 Å, similar to that at the interface.

[4]We assume that both μ^* and $\omega_{\log}$ are not the relevant factors that make the difference between interfacial and bulk superconductivity. Regarding the phonon frequencies, similar values have been reported for bulk doped BBO [14,29].

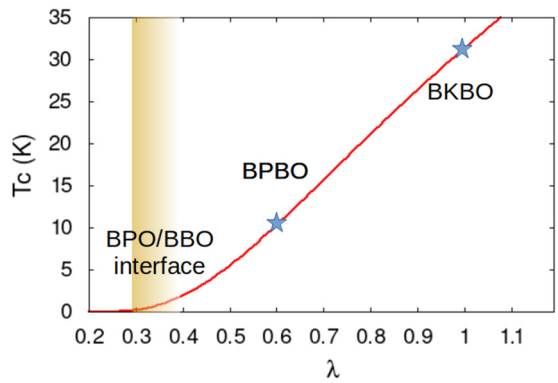

FIG. 4. Schematic evolution of T_c for the BBO family of superconductors according to the McMillan modified equation.

because the electronic structure remains similar. The system seems to bear lower level of doping when Pb substitutes Bi. Contrary to what happens at the BPO/BBO interface, in the bulk cases, there is a small DOS at E_F and the high T_c has its origin in the large coupling matrix elements of the three phonon modes.

In a previous work, it has been predicted by means of DFT calculations that the (001) BBO surface should become metallic if a Bi termination is achieved [16]. The mechanism behind this effect should be intrinsic and has to do with the breaking of charge ordering at the two outermost layers due to the incomplete oxygen environment of the surface ions. Moreover, in view of the observed electronic and structural reconstruction of BiO_2 surface, it has been claimed that the predicted 2D electron gas deserved further investigation regarding its superconducting properties. We believe that the physics at the BPO/BBO interface is related to the one described for the Bi-terminated (001) BBO surface. In both cases, there is electronic and structural reconstruction due to a sudden change in the oxygen octahedra environment of the charge ordered Bi ions.

In particular, at the BPO/BBO interface there is a partial suppression of the BBO charge order due to the breaking of the translation symmetry along the z direction by the presence of the BPO layer. There are two types of electronic states at the interface, the sp-Pb electron doping bands and the s-Bi ones. The former are more spatially extended while the last ones are 2D. In this work, we show that the 2D interfacial states present a substantial electron-phonon coupling with the stretching modes and are responsible for the mechanism behind the experimentally observed 2D superconductivity at the BPO/BBO bilayer. These results should encourage future work to search different ways to break the charge ordered phases at interfaces with semiconductors like BBO, for instance, to involve also the Bi^{+5} empty bands. This would imply an intrinsic breaking of charge order at the interface that might be achieved if the top material had less tendency to metallicity than Pb. We also suggest that electrostatic doping is another interesting possibility to be explored.

The authors receive financial support from Grant No. PIP2015-2017 112-201501-00364-CO of CONICET and from Grant No. PICT-2015-0869 and PICT-2019-02128 of the ANPCyT, Argentina.

[1] N. Reyren, S. Thiel, A. D. Caviglia, L. F. Kourkoutis, G. Hammerl, C. Richter, C. W. Schneider, T. Kopp, A.-S. Rüetschi, D. Jaccard *et al.*, Science **317**, 1196 (2007).
[2] A. Gozar, G. Logvenov, L. F. Kourkoutis, A. T. Bollinger, L. A. Giannuzzi, D. A. Muller, and I. Bozovic, Nature (London) **455**, 782 (2008).
[3] G. Logvenov, A. Gozar, and I. Bozovic, Science **326**, 699 (2009).
[4] A. K. Pedersen, S. Ichinokura, T. Tanaka, R. Shimizu, T. Hitosugi, and T. Hirahara, Phys. Rev. Lett. **124**, 227002 (2020).
[5] B. Meir, S. Gorol, T. Kopp, and G. Hammerl, Phys. Rev. B **96**, R100507(R) (2017).
[6] R. J. Cava, B. Batlogg, J. J. Krajewski, R. Farrow, L. W. Rupp, A. E. White, K. Short, W. F. Peck, and T. Kometani, Nature (London) **332**, 814 (1988).
[7] A. W. Sleight, J. L. Gillson, and P. E. Bierstedt, Solid State Commun. **17**, 27 (1975).
[8] L. F. Mattheiss and D. R. Hamann, Phys. Rev. B **28**, 4227 (1983).
[9] C. Franchini, A. Sanna, M. Marsman, and G. Kresse, Phys. Rev. B **81**, 085213 (2010).
[10] L. F. Mattheiss and D. R. Hamann, Phys. Rev. B **26**, 2686 (1982).
[11] L. F. Mattheiss and D. R. Hamann, Phys. Rev. Lett. **60**, 2681 (1988).
[12] D. Cox and A. Sleight, Solid State Commun. **19**, 969 (1976).
[13] C. H. P. Wen, H. C. Xu, Q. Yao, R. Peng, X. H. Niu, Q. Y. Chen, Z. T. Liu, D. W. Shen, Q. Song, X. Lou *et al.*, Phys. Rev. Lett. **121**, 117002 (2018).
[14] Z. P. Yin, A. Kutepov, and G. Kotliar, Phys. Rev. X **3**, 021011 (2013).
[15] W. Fu, D. Visser, K. Knight, and D. IJdo, J. Solid State Chem. **180**, 1559 (2007).
[16] V. Vildosola, F. Güller, and A. M. Llois, Phys. Rev. Lett. **110**, 206805 (2013).
[17] J. Heyd, G. E. Scuseria, and M. Ernzerhof, J. Chem. Phys. **118**, 8207 (2003).
[18] A. V. Krukau, O. A. Vydrov, A. F. Izmaylov, and G. E. Scuseria, J. Chem. Phys. **125**, 224106 (2006).
[19] G. Kresse and J. Furthmüller, Phys. Rev. B **54**, 11169 (1996).
[20] G. Kresse and D. Joubert, Phys. Rev. B **59**, 1758 (1999).
[21] See Supplemental Material at http://link.aps.org/supplemental/10.1103/PhysRevB.103.174509 for technical details.
[22] T. Thonhauser and K. M. Rabe, Phys. Rev. B **73**, 212106 (2006).
[23] R. F. W. Bader, Chem. Rev. **91**, 893 (1991).
[24] J. P. Perdew, K. Burke, and M. Ernzerhof, Phys. Rev. Lett. **77**, 3865 (1996).

[25] B. Yan, M. Jansen, and C. Felser, Nat. Phys. **9**, 709 (2013).
[26] G. Li, B. Yan, R. Thomale, and W. Hanke, Sci. Rep. **5**, 10435 (2015).
[27] M. M. Dacorogna, M. L. Cohen, and P. K. Lam, Phys. Rev. Lett. **55**, 837 (1985).
[28] A. I. Liechtenstein, I. I. Mazin, C. O. Rodriguez, O. Jepsen, O. K. Andersen, and M. Methfessel, Phys. Rev. B **44**, 5388 (1991).
[29] V. Meregalli and S. Y. Savrasov, Phys. Rev. B **57**, 14453 (1998).
[30] W. L. McMillan, Phys. Rev. **167**, 331 (1968).